

# Quantum autoencoders with enhanced data encoding

Carlos Bravo-Prieto<sup>1,2</sup>

<sup>1</sup>Departament de Física Quàntica i Astrofísica and Institut de Ciències del Cosmos (ICCUB), Universitat de Barcelona, Martí i Franquès 1, 08028 Barcelona, Spain.

<sup>2</sup>Technology Innovation Institute, Abu Dhabi.

We present the enhanced feature quantum autoencoder, or EF-QAE, a variational quantum algorithm capable of compressing quantum states of different models with higher fidelity. The key idea of the algorithm is to define a parameterized quantum circuit that depends upon adjustable parameters and a feature vector that characterizes such a model. We assess the validity of the method in simulations by compressing ground states of the Ising model and classical handwritten digits. The results show that EF-QAE improves the performance compared to the standard quantum autoencoder using the same amount of quantum resources, but at the expense of additional classical optimization. Therefore, EF-QAE makes the task of compressing quantum information better suited to be implemented in near-term quantum devices.

## I. INTRODUCTION

Large-scale fault-tolerant quantum computation is a rather distant dream, typically estimated to be a few decades ahead. A reasonable question then is whether we can do something useful with the existing noisy intermediate-scale quantum (NISQ) [1] computers. The main proposal is to use them as a part of a hybrid classical-quantum device. The variational quantum algorithms (VQAs) are a class of algorithms that use such hybrid devices, which manage to reduce the requisites of quantum computational resources at the expense of classical computation.

The general rationale of a VQA is to define a parametrized quantum circuit whose architecture is dictated by the type and size of the quantum computer that is available. This quantum circuit, in turn, will depend on a set of classical parameters that can be adjusted using a quantum-classical optimization loop by minimizing a cost function. In this manner, we look for a quantum circuit that allows to perform a particular task, given the available quantum resources. Several VQAs have already been proposed in the context of making NISQ computers practically useful for real applications [2–15].

Lately, much attention has been paid to data encoding in VQAs [16, 17]. Indeed, it was proven that data encoded into the model influences the expressive power of parameterized quantum circuits [18]. Specifically, this idea has been implemented for classification of data [19, 20], and very recently, to study energy profiles of quantum Hamiltonians [21]. Here, we introduce this concept to the Quantum Autoencoder (QAE) [7], a VQA designed to compress the input quantum information through a smaller latent space. In this scheme, we look for a parameterized

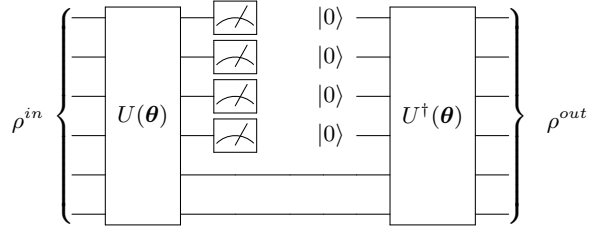


FIG. 1. Circuit implementation of a quantum autoencoder with a 2-qubit latent space. The unitary  $U(\theta)$  encodes a 6-qubit input state  $\rho^{in}$  into a 2-qubit intermediate state, after which the decoder  $U^\dagger(\theta)$  attempts to reconstruct the input, resulting in the output state  $\rho^{out}$ .

quantum circuit  $U(\theta)$  that encodes an initial input state into an intermediate latent space, after which the action of the decoder,  $U^\dagger(\theta)$ , attempts to reconstruct the input. A graphical depiction of a QAE is shown in Fig. 1.

Note that the motivation for a quantum autoencoder is to be able to recognize patterns beyond the capabilities of a classical autoencoder, given the different properties of quantum mechanics. Moreover, recall that for NISQ devices, any tool that can reduce the amount of quantum resources can be considered valuable. For instance, quantum autoencoders could be used as a state preparation engine in the context of other VQAs. That is, we could combine, say, a Variational Quantum Eigensolver [2] with a pretrained QAE, where now the only active parameters are associated with the latent space.

In the following, we present the enhanced feature quantum autoencoder (EF-QAE). As we will see, its key ingredient is to define a parameterized quantum circuit that depends upon adjustable parameters and a feature vector that characterizes the model we aim to compress.

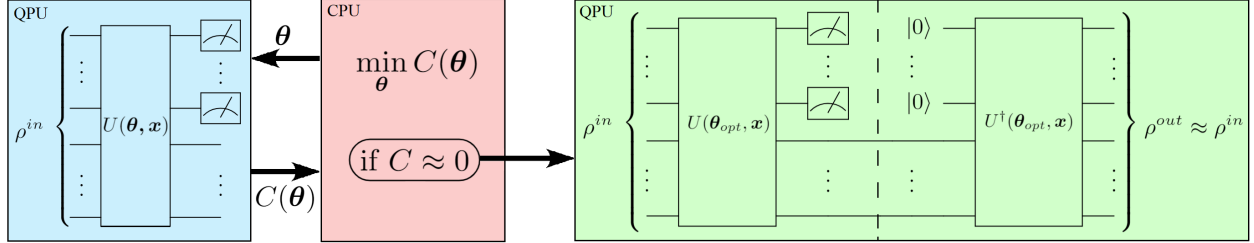


FIG. 2. Schematic representation of the EF-QAE. The input to EF-QAE is a set of initial states  $\rho^{in}$ , a feature vector  $\mathbf{x}$  that characterizes the initial states, and a shallow sequence of quantum gates  $U$ . The feature vector  $\mathbf{x}$  is encoded together with the variational parameters  $\theta$ , where the latter are adjusted in a quantum-classical optimization loop until the local cost  $C(\theta)$  converges to a value close to 0. When this loop terminates and the optimal parameters  $\theta_{opt}$  are found, the resulting circuit  $U(\theta_{opt}, \mathbf{x})$  prepares compressed states  $|\phi\rangle$  of a particular model. Moreover, we may apply  $U^\dagger(\theta_{opt}, \mathbf{x})|0\dots0\rangle \otimes |\phi\rangle$  to recover  $\rho^{out} \approx \rho^{in}$ .

## II. EF-QAE ALGORITHM

### A. Overview

Here, we present the enhanced feature quantum autoencoder (EF-QAE). A schematic diagram of the EF-QAE can be seen in Fig. 2. The algorithm can be initialized with a set of initial states  $\rho_i^{in}$ , a feature vector  $\mathbf{x}$ , and a shallow sequence of quantum gates  $U$ . In this scheme, we define a unitary  $U(\theta, \mathbf{x})$  acting on the initial state  $\rho_i^{in}$ , where  $\mathbf{x}$  is a feature vector that characterizes the set of input states. For instance, as we will see in Sec. III,  $\mathbf{x}$  may be the transverse field  $\lambda$  of the 1D Ising spin chain. Once the trial state is prepared, measurements are performed to evaluate the cost function  $C(\theta)$ . This result is then fed into the classical optimizer, where the parameters  $\theta$  are adjusted in a quantum-classical loop until the cost function converges to a value close to 0. When the loop terminates,  $U(\theta_{opt}, \mathbf{x})$  prepares compressed states  $|\phi\rangle$  of a particular model.

### B. Cost function

The quantum information of the input state through the smaller latent space must be stored. Therefore, it is important to quantify how well the information is preserved in the compressed state  $|\phi\rangle$ . This is generally quantified by a cost function that one has to minimize. In Ref. [7], this cost function is not constructed from local operators, and therefore it may lead to trainability issues even for shallow depth quantum circuits [22, 23].

Here, however, we use a cost function designed from local operators [23]. A figure of merit for the wrong answer when training is simply the to-

tal amount of non-zero measurement outcomes on the  $n_t$  trash qubits, which will be minimized. To design the cost function to be local, different outcomes may be penalized by their Hamming distance to the  $|0\rangle^{\otimes n_t}$  state, which is just the number of symbols that are different in the binary representation. Thus, the local cost function  $C$  to be minimized simply is

$$C \equiv \sum_{k,j} d_H M_{k,j} \equiv \frac{1}{2} \sum_{k=1}^{n_t} (1 - \langle Z_k \rangle), \quad (1)$$

where  $d_H$  denotes the Hamming distance and  $M_{k,j}$  are the results of the  $j$ -th measurement on the  $k$  trash qubit in the computational basis. Equivalently, it can also be defined in terms of local  $Z$  Pauli operators. We may now apply classical optimization techniques to find the optimal parameters that provide exact output coincidence to the  $|0\rangle^{\otimes n_t}$  state on the trash qubits. Finally, notice that this cost function delivers direct information on how the compression of the trash qubits is performed, and has a zero value if and only if the compression is completed.

### C. Ansatz

To implement the EF-QAE model on a quantum computer, we must define the form of the parametrized unitary  $U(\theta, \mathbf{x})$ , decomposing it into a quantum circuit suitable for optimization. Recall that a quantum autoencoder may be thought of as a disentangling unitary. The complexity of the circuit thus limits this property. Given the limited available quantum resources in practice, due to the coherence times and gate errors, we will look for a circuit structure that maximally exploits entanglement while maintaining a shallow depth.

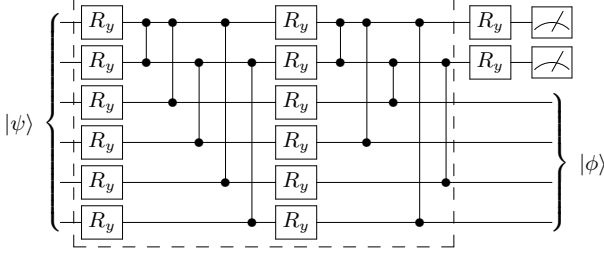


FIG. 3. Variational quantum ansatz employed for the EF-QAE model. As indicated by the dashed box, each layer is composed of  $CZ$  gates acting on the trash qubits preceded by  $R_y$  qubit rotations,  $R_y(\theta_j) = e^{-i\theta_j Y/2}$ . A cascade of  $CZ$  gates is then applied between the trash qubits and the qubits containing the final compressed state. After implementing the layered ansatz, a final layer of  $R_y$  qubit gates is applied to the trash qubits. Note that the sequence of entangling gates can be applied mostly in parallel.

A primitive strategy to construct a variational circuit in a more general case may consist of building a circuit of arbitrary 2- and 1-qubit gates characterized by some parameters. However, this is a naive approach. The action of the EF-QAE on the original state is

$$U|\psi\rangle = |0\rangle \otimes \dots \otimes |0\rangle \otimes |\phi\rangle. \quad (2)$$

Thus, it is clear that the entangling gates should mostly act between each of the trash qubits, and between the trash qubits and the qubits containing the final compressed state. Subsequently, we may avoid using entangling gates between the qubits that are not trash while maximizing the entangling gates on the ones of interest. This could be done using a similar structure to that depicted in Fig. 3. Notice that most of the sequence of entangling gates can be applied in parallel at the same step.

We now encode the feature vector  $\mathbf{x}$  into each of the single  $R_y$  qubit rotations by using a linear function as

$$R_y^{(i,j)}(\boldsymbol{\theta}, \mathbf{x}) = R_y\left(\theta^{(i)}x^{(j)} + \theta^{(i+1)}\right), \quad (3)$$

where  $i, j$  simply indicates a component of the vector, and  $\boldsymbol{\theta}$  are the parameters adjusted in the optimization loop.

### III. 1D ISING SPIN CHAIN

The EF-QAE can be verified on simulations. We utilized the open-source Python API Qibo [24, 25]

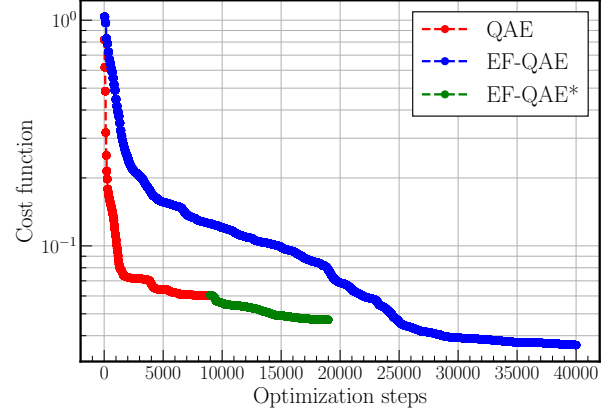


FIG. 4. Cost function value as a function of the number of optimization steps. Here, we consider the standard QAE, EF-QAE, and EF-QAE\*. The EF-QAE\* is the EF-QAE initialized with the optimal parameters of QAE. The EF-QAE achieves twice the compression of the QAE using the same quantum resources, at the expense of additional classical optimization.

for the simulation of the quantum circuits. Here, we benchmark both the EF-QAE and the standard QAE in the case of a paradigmatic quantum spin chain with 6 qubits, the transverse field Ising model. The 1D Ising model is described by the following Hamiltonian

$$H_{Ising} = \sum_j \sigma_j^z \sigma_{j+1}^z + \lambda \sum_j \sigma_j^x, \quad (4)$$

where  $\lambda$  is the transverse field. In the thermodynamic limit, the system has a quantum phase transition exactly at  $\lambda = 1$ .

The EF-QAE and QAE are optimized over a training set of ground states of the Ising model. Specifically, we have considered  $N=20$  equispaced ground states in between  $\lambda = 0.5$  and  $\lambda = 1.0$ , with initial random parameters. For the cost function, we computed Eq. 1 for each training state and then averaged them as

$$C_N = \frac{\sum_N C}{N}. \quad (5)$$

Nonetheless, notice that for other models, sophisticated cost functions could be more convenient to implement. We have considered the variational quantum circuit in Fig. 3 with 3 layers, and therefore, the resulting compressed state contains 4 qubits. Note that the feature vector  $\mathbf{x}$  for the EF-QAE is simply a scalar that takes the value of the transverse field  $\lambda$ . Lastly, the classical technique employed in the optimization loop is the BFGS method.

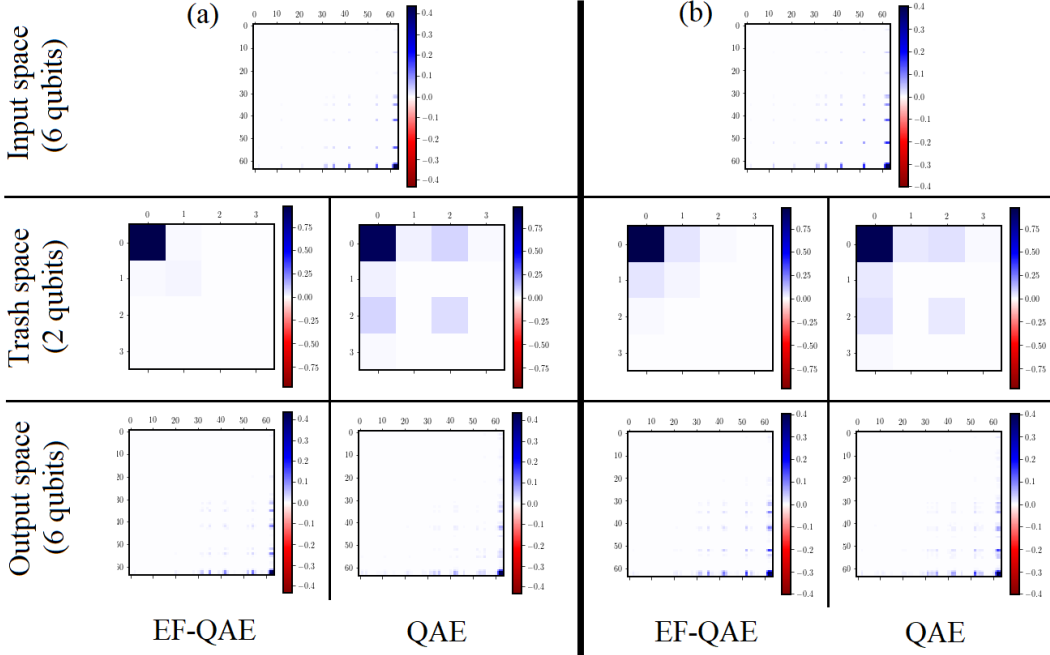


FIG. 5. Visualization of the input space, trash space, and output space for the EF-QAE and QAE, considering two different test ground states of the 1D Ising model corresponding to (a)  $\lambda = 0.60$  and (b)  $\lambda = 0.75$ . The size of the registers appears within parenthesis (number of qubits). The spaces are characterized as the density matrices of the input, trash and output states. Integer labels denote the binary representation of the computational basis states.

In Fig. 4, we show the cost function value as a function of the number of optimization steps. The EF-QAE\* is simply the EF-QAE initialized with the optimal parameters of QAE. This way, the EF-QAE\* will always improve the QAE performance. As can be seen, the EF-QAE achieves twice the compression of the QAE using the same quantum resources. Notice, however, that the EF-QAE contains twice as many variational parameters, and therefore, the increase in performance is at the expense of additional classical optimization.

To quantify these expectations, we assess both EF-QAE and QAE with the optimal parameters against two test ground states of the Ising model, specifically, with  $\lambda = 0.60$  and  $\lambda = 0.75$ . The results are shown in Fig. 5. Here, we show a density matrix visualization of the input, trash, and output state. The EF-QAE achieves better compression to the  $|00\rangle$  trash state, and therefore, higher fidelity on the output state. As we change the values of the transverse field, we note that the compression differs. Both cases considered, however, the performance of the EF-QAE is preferable.

#### IV. HANDWRITTEN DIGITS

In this section, we benchmark EF-QAE and QAE models in the case of  $8 \times 8$  handwritten digit compression with 6 qubits using 4 layers. The data comprising each digit consists of a matrix with values from 0 to 16 corresponding to a gray map. Each value of this matrix is encoded in the amplitude of a 6-qubit state, further restricted to normalization.

The EF-QAE and QAE are optimized over a training set of handwritten digits obtained from the Python package `Scikit Learn` [26]. Specifically, we have considered  $N=20$  handwritten digits, 10 of each corresponding to **0** or **1**. The simulation details are equivalent to those in Sec. III. Here, the feature vector for the EF-QAE corresponds to  $\mathbf{x} = (1, 2)$ . That is, we simply input a value of  $x = 1$  ( $x = 2$ ) if the handwritten digit corresponds to **0** (**1**). The rationale behind choosing  $\mathbf{x} = (1, 2)$  is that no obvious feature distinguishes both digits. Nonetheless, more convenient strategies could be used in future work. For instance, one may allow the feature vector  $\mathbf{x}$  to be a free variational parameter.

In Fig. 6, we show the cost function value as a function of the number of optimization steps. Re-

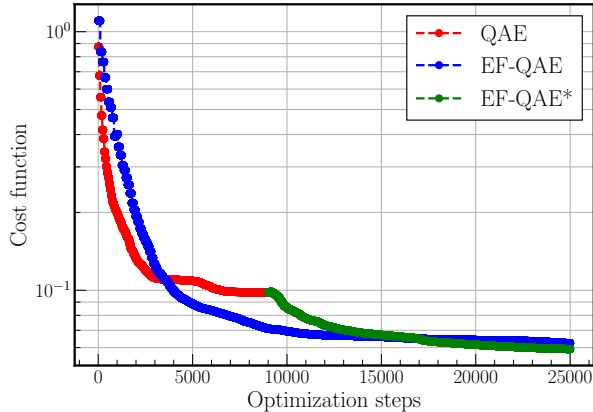


FIG. 6. Cost function value as a function of the number of optimization steps. Here, we consider the standard QAE, EF-QAE, and EF-QAE\*. The EF-QAE\* is the EF-QAE initialized with the optimal parameters of QAE. The EF-QAE achieves three times the compression of the QAE using the same quantum resources, at the expense of additional classical optimization.

call that EF-QAE\* is simply the EF-QAE initialized with the optimal parameters of QAE. The behavior is similar to the one observed in the case of the Ising model, where the EF-QAE achieves three times the compression of the QAE using the same quantum resources.

Once again, to gain insight into the compression process, we assess both EF-QAE and QAE with the optimal parameters against two handwritten test digits corresponding to **0** and **1**. The results are shown in Fig. 7. Here, we plot the output digit of the EF-QAE and QAE. Once more, since EF-QAE achieves better compression to the  $|00\rangle$  trash state, we obtain higher fidelity on the output state. Remarkably, in both cases, the performance of the EF-QAE is improved with respect to the QAE.

## V. DISCUSSION

We have presented a variational quantum algorithm called EF-QAE capable of compressing quantum data of a parameterized model. In contrast to standard QAE, EF-QAE achieves this compression with higher fidelity. Its key idea is to define a parameterized quantum circuit that depends upon adjustable parameters and a feature vector that characterizes such a model.

We have validated the EF-QAE in simulations by compressing ground states of the 1D Ising spin chain,

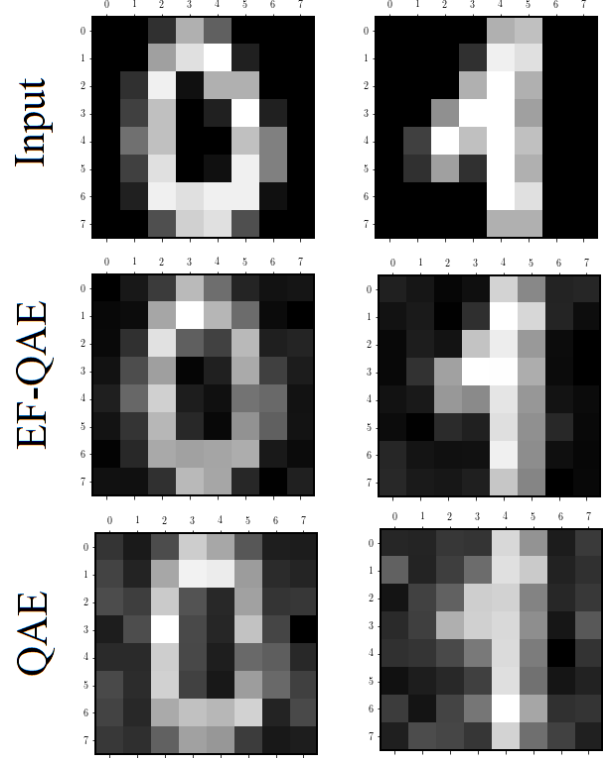


FIG. 7. Images of **0** and **1** handwritten test digits encoded into a 6-qubit state ( $8 \times 8$  pixels). Images shown correspond to the input state, and the output states of the EF-QAE and QAE models. As can be seen, the fidelity of the EF-QAE output state is improved compared to QAE.

and classical handwritten digits encoded into quantum states. We compared the results with the standard QAE. The results show that EF-QAE achieves better compression of the initial state, and therefore, the final output state is recovered with higher fidelity. Moreover, the learning task of EF-QAE can be initialized with the optimal QAE parameters. In this manner, EF-QAE will always improve the QAE performance. Nonetheless, the encoding strategy of the feature vector is amenable to be improved, for instance, using a non-linear encoding or allowing the feature vector to be a free variational parameter.

On the counterpart, EF-QAE needs additional classical optimization compared to QAE. However, in contrast, we increase the compression performance using the same amount of limited quantum resources. In this sense, EF-QAE is a step toward what could be done on NISQ computers, shortening the distance between current quantum devices and practical applications.

## CODE AVAILABILITY

The code is available in Github [27].

## ACKNOWLEDGEMENTS

The author would like to thank Diego García-Martín and José I. Latorre for fruitful discussions.

This work is supported by the projects PGC2018-095862-B-C22 and Quantum CAT 001-P-001644.

---

[1] J. Preskill, *Quantum* **2**, 79 (2018).

[2] A. Peruzzo, J. McClean, P. Shadbolt, M.-H. Yung, X.-Q. Zhou, P. J. Love, A. Aspuru-Guzik, and J. L. O’Brien, *Nature Communications* **5**, 4213 (2014).

[3] C. Kokail, C. Maier, R. van Bijnen, T. Brydges, M. K. Joshi, P. Jurcevic, C. A. Muschik, P. Silvi, R. Blatt, C. F. Roos, and P. Zoller, *Nature* **569**, 355 (2019).

[4] O. Higgott, D. Wang, and S. Brierley, *Quantum* **3**, 156 (2019).

[5] T. Jones, S. Endo, S. McArdle, X. Yuan, and S. C. Benjamin, *Physical Review A* **99**, 062304 (2019).

[6] Y. Li and S. C. Benjamin, *Physical Review X* **7**, 021050 (2017).

[7] J. Romero, J. P. Olson, and A. Aspuru-Guzik, *Quantum Science and Technology* **2**, 045001 (2017).

[8] S. Khatri, R. LaRose, A. Poremba, L. Cincio, A. T. Sornborger, and P. J. Coles, *Quantum* **3**, 140 (2019).

[9] R. LaRose, A. Tikku, É. O’Neel-Judy, L. Cincio, and P. J. Coles, *npj Quantum Information* **5**, 1 (2018).

[10] C. Bravo-Prieto, D. García-Martín, and J. I. Latorre, *Physical Review A* **101**, 062310 (2020).

[11] C. Bravo-Prieto, R. LaRose, M. Cerezo, Y. Subasi, L. Cincio, and P. J. Coles, arXiv:1909.05820 (2019).

[12] C. Cirstoiu, Z. Holmes, J. Iosue, L. Cincio, P. J. Coles, and A. Sornborger, *npj Quantum Information* **6**, 1 (2020).

[13] J. Carolan, M. Mohseni, J. Olson, M. Prabhu, C. Chen, D. Bunandar, Y. Niu, N. Harris, F. Wong, M. Hochberg, S. Lloyd, and D. Englund, *Nature Physics* **95**, 1 (2020).

[14] S. McArdle, T. Jones, S. Endo, Y. Li, S. C. Benjamin, and X. Yuan, *npj Quantum Information* **5**, 1 (2019).

[15] S. Endo, J. Sun, Y. Li, S. C. Benjamin, and X. Yuan, *Physical Review Letters* **125**, 010501 (2020).

[16] S. Lloyd, M. Schuld, A. Ijaz, J. Izaac, and N. Killoran, arXiv:2001.03622 (2020).

[17] R. LaRose and B. Coyle, *Physical Review A* **102**, 032420 (2020).

[18] M. Schuld, R. Sweke, and J. J. Meyer, arXiv:2008.08605 (2020).

[19] V. Havlíček, A. D. Córcoles, K. Temme, A. W. Harrow, A. Kandala, J. M. Chow, and J. M. Gambetta, *Nature* **567**, 209 (2019).

[20] A. Pérez-Salinas, A. Cervera-Lierta, E. Gil-Fuster, and J. I. Latorre, *Quantum* **4**, 226 (2020).

[21] A. Cervera-Lierta, J. S. Kottmann, and A. Aspuru-Guzik, arXiv:2009.13545 (2020).

[22] J. R. McClean, S. Boixo, V. N. Smelyanskiy, R. Babbush, and H. Neven, *Nature Communications* **9**, 4812 (2018).

[23] M. Cerezo, A. Sone, T. Volkoff, L. Cincio, and P. J. Coles, arXiv:2001.00550 (2020).

[24] S. Efthymiou, S. Ramos-Calderer, C. Bravo-Prieto, A. Pérez-Salinas, D. García-Martín, A. García-Saez, J. I. Latorre, and S. Carrazza, “Quantum-TII/qibo on Github,” Zenodo, DOI:10.5281/zenodo.3997194 (2020).

[25] S. Efthymiou, S. Ramos-Calderer, C. Bravo-Prieto, A. Pérez-Salinas, D. García-Martín, A. García-Saez, J. I. Latorre, and S. Carrazza, arXiv:2009.01845 (2020).

[26] F. Pedregosa, G. Varoquaux, A. Gramfort, V. Michel, B. Thirion, O. Grisel, M. Blondel, P. Prettenhofer, R. Weiss, V. Dubourg, J. Vanderplas, A. Passos, D. Cournapeau, M. Brucher, M. Perrot, and E. Duchesnay, *Journal of Machine Learning Research* **12**, 2825 (2011).

[27] [https://github.com/Quantum-TII/qibo/tree/master/examples/EF\\_QAE](https://github.com/Quantum-TII/qibo/tree/master/examples/EF_QAE).

[28] K. Sharma, S. Khatri, M. Cerezo, and P. Coles, *New Journal of Physics* **22**, 043006 (2020).

## Appendix A: Resilience to noise

It has been shown recently that specific VQAs can exhibit noise resilience [28]. That is, the optimal parameters are unaffected by certain noise models. Here we prove that the local cost function  $C$  is resilient to global depolarizing noise. Let us rewrite  $C$

from Eq. 1 as

$$C = \frac{1}{2} \sum_{k=1}^{n_t} (1 - \zeta^{(k)}) , \quad (\text{A1})$$

where  $\zeta^{(k)} = \langle 0 | U^\dagger (Z_k \otimes \mathbb{1}_{\bar{k}}) U | 0 \rangle$ . From now on, we refer to  $\tilde{C}$  and  $\tilde{\zeta}$  as the noisy versions of these quantities. Recall that global depolarizing noise transforms the state according to  $\rho \rightarrow q\rho + (1-q)\mathbb{1}/d$ . If we consider a circuit that has depth  $D$ , then the final state is  $q^D \rho + (1-q^D)\mathbb{1}/d$ . Notice as well that  $\tilde{\zeta}^{(k)}$  is estimated simply by executing the circuit in Fig. 3 and measuring in the computational basis. The maximally mixed state has zero expectation value, since we measure Pauli  $Z$  operators. Therefore, we obtain that  $\tilde{\zeta}^{(k)} = q^D \zeta^{(k)}$ , where  $D$  is the depth of the circuit used to estimate  $\zeta^{(k)}$ . This implies

$$\tilde{C} = \frac{1}{2} \sum_{k=1}^{n_t} (1 - q^D \zeta^{(k)}) . \quad (\text{A2})$$

From this expression, we see that

$$\arg \min_{\theta} \tilde{C} = \arg \max_{\theta} \left( \sum_{k=1}^{n_t} \zeta^{(k)} \right) . \quad (\text{A3})$$

It is clear as well that

$$\arg \min_{\theta} C = \arg \max_{\theta} \left( \sum_{k=1}^{n_t} \zeta^{(k)} \right) . \quad (\text{A4})$$

Hence we arrive at

$$\arg \min_{\theta} \tilde{C} = \arg \min_{\theta} C . \quad (\text{A5})$$

This proves our statement of global depolarizing noise resilience, since it shows that the optimal parameters are unaffected.